Available online at www.sciencedirect.com
SCIENCE DIRECT®
Journal of Magnetic Resonance 166 (2004) 190–201
JMR Journal of Magnetic Resonance
www.elsevier.com/locate/jmr

Amide proton relaxation measurements employing a highly deuterated protein☆

Tobias S. Ulmer,*,[1] Iain D. Campbell, and Jonathan Boyd*

Department of Biochemistry, University of Oxford, South Parks Road, Oxford OX1 3QU, UK

Received 20 August 2003; revised 14 October 2003

Abstract

Proton NMR longitudinal and transverse relaxation rates of unlabelled proteins are generally dominated by the many ^1H–^1H dipolar interactions so that *spin diffusion*, rather than molecular or internal motions, governs longitudinal relaxation. Here, relaxation measurements of backbone amide proton ($^1H^N$) magnetisations have been carried out employing the 99% ^2H, 98% ^{15}N labelled, small $^2F2$ protein domain in 10%/90% H_2O/D_2O solution. Under these conditions, the longitudinal relaxation rates exhibit time constants, $T_1^* = 1/R_1^*$ if described by a mono-exponential, within the range of 3.0 to 18.7 s—a wide range which indicates that the phenomenon of *spin diffusion* has been greatly reduced. The majority of $^1H^N$ nuclei in this sample (pH 4.0 and 5 °C) exhibit chemical exchange with solvent that couples their longitudinal relaxation to that of the solvent. For the subset of $^1H^N$ nuclei not undergoing detectable solvent chemical exchange, the R_1^* rates correlate well with their individual $^1H^{N,O}/^2H^{N,O}$ structural environments. The correlation for corresponding transverse relaxation rates, R_2^* was found to be less good. Longitudinal relaxation measurements in 1%/99% H_2O/D_2O solution identify a further subset of $^1H^N$ nuclei which exhibit essentially indistinguishable R_1^* rates in both 1% and 10% H_2O, implying that averaging of rates from *spin diffusion* processes and different $^2F2$ isotopomer populations are negligible for these $^1H^N$ sites. In addition to a high sensitivity to structural parameters, model calculations predict $^1H^N$ relaxation rates to exhibit pronounced sensitivity to internal dynamics.

Keywords: Cross-relaxation; Deuteration; Protein dynamics; Proton relaxation; Spin diffusion

1. Introduction

The dynamics and plasticity of proteins are important aspects of their structure and function [1–3]. The high sensitivity of NMR parameters to dynamic processes over a wide range of timescales [4–6] and the relatively large number of reporter sites makes the analysis of protein dynamics by NMR particularly powerful. The usual first choice in NMR relaxation studies is the backbone ^{15}N nucleus, whose relaxation is governed by ^{15}N chemical shielding anisotropy (CSA) and $^1H^N$–^{15}N dipole–dipole interactions [7]. When employing ^{13}C isotopic enrichment, the interpretation of ^{13}C relaxation rates is complicated by the presence of $^1J_{CC}$ couplings and the many ^{13}C–^{13}C dipolar interactions, which lead to cross-relaxation between ^{13}C nuclei. For ^1H spin relaxation, e.g., of the backbone amide proton ($^1H^N$), interpretation is particularly difficult because of the efficient relayed transfer of magnetisation over several spins (*spin diffusion*) and the ensuing uncertainties about the source of relaxation in a dense ^1H system [8]. Nevertheless, it is appealing to explore $^1H^N$ relaxation since, in principle, information about segmental backbone, e.g., H^N–H^N, and backbone-side chain, e.g. H^N–H^C, dynamics may be obtained. These studies might complement the use of deuterium spins as probes for side-chain dynamics [9,10].

In protonated proteins (natural ^1H abundance) *spin diffusion*, rather than molecular or internal motions, appears to be the primary mechanism governing longitudinal relaxation [8]. This leads to averaged and relatively

☆ Supplementary data associated with this article can be found at doi: 10.1016/S1090-7807(03)00349-5.

* Corresponding authors. Fax: +1-301-496-0825.
E-mail addresses: tobias.ulmer@nih.gov (T.S. Ulmer), jonathan.boyd@bioch.ox.ac.uk (J. Boyd).
[1] Present addresses: Laboratory of Chemical Physics, National Institute of Diabetes and Digestive and Kidney Diseases, National Institutes of Health, Bethesda, MD 20892, USA.

1090-7807/$ - see front matter © 2003 Elsevier Inc. All rights reserved.
doi:10.1016/j.jmr.2003.10.012

uniform longitudinal relaxation rates because fast relaxing spins provide relaxation sinks for slower ones [8]. For these reasons, proton relaxation has been used relatively rarely. Deuteration has been employed to simplify protein NMR spectra for many years [11,12] with several recent applications to larger proteins and protein-ligand complexes [13–16]. Deuteration is also widely used to prolong the transverse relaxation times of ^{1}H–X dipolar-coupled heteronuclei and solvent-exchangeable $^1H^N$ nuclei in structural studies of larger proteins [17–19]. These studies take advantage of the approximately 6.5 times lower gyromagnetic ratio of the deuteron compared to the proton and the elimination of ^{1}H–^{1}H scalar couplings, in particular $^3J_{HNH\alpha}$. Another important application is the identification of conformational exchange contributions to $^1H^N$ transverse relaxation in deuterated proteins [20]. Due to the efficient quadrupolar relaxation of deuterons [21], the self-relaxation of ^{2}H in a small globular protein will be on the order of 20 ms, which is too short to allow significant cross-relaxation with protons to occur. Thus, deuteration helps to "insulate" protons from each other by eliminating relay partners in the usual spin diffusion network. Reduced spin diffusion offers the potential to use relatively long NOESY mixing times and, thus, collection of longer range interproton distance restraints [22–24]. Excluding solvent exchange processes, the longitudinal relaxation rates are expected to be dominated by high frequency motions.

The present study seeks to take advantage of the benefits of deuterium labelling in the analysis of longitudinal and transverse relaxation characteristics of the backbone amide protons ($^1H^N$). In particular, the potential for obtaining site-specific longitudinal relaxation rates is examined. The protein under examination is the 59-residue second type 2 domain from fibronectin (^{2}F2) of which >99% of all non-exchangeable protons (H^C) were replaced with deuterons in addition to enrichment in ^{15}N. The solvent exchangeable protons (H^N and H^O) comprise 26% of all ^{2}F2 protons and the ^{2}H/^{1}H ratio in this fraction was set to 10% or 1%, by changing the isotope composition of the solvent. A subset of eleven $^1H^N$ nuclei could be identified for which chemical exchange with solvent was negligible. Of this subset (at least) five $^1H^N$ nuclei exhibited longitudinal relaxation rates (in non-selective inversion recovery experiments) that were indistinguishable in 1%/99% and 10%/90% H_2O/D_2O solution, indicating the absence of significant averaging effects.

2. Experimental procedures

2.1. Protein production and NMR sample preparation

The 59-residue second type 2 domain of human fibronectin (^{2}F2), residues 375–433, carrying a single *N*-acetylglucosamine (GlcNAc) unit N-linked to N25, was produced by recombinant expression from the methylotrophic yeast *P. pastoris* as described [25,26]. (98% $^{15}ND_4)_2SO_4$, D_2O and, initially, glycerol-d_8 were used as metabolites. After consumption of the glycerol-d_8 production of protein is induced using methanol-d_4 as the sole carbon source.

Two NMR samples, termed A and B, were prepared. The pH of the samples was adjusted to 4.0 (uncorrected pH meter reading) with predefined amounts of aqueous NaOH to achieve the desired H_2O/D_2O ratio. For sample A, freeze-dried ^{2}F2 was dissolved in 10%/90% H_2O/D_2O solution to a concentration of 2 mM. For sample B, ^{2}F2 was dissolved in 1%/99% H_2O/D_2O solution to a concentration of 2 mM. The samples were degassed by three freeze-pump-thaw cycles in the NMR tube (Wilmad 542-PP-8) and subsequently flame-sealed. The preparation of sample A was repeated to assess the reproducibility of the sample preparation and measurement scheme.

^{2}F2 contains 323 non-exchangeable H^C, 15 exchangeable H^O and 100 exchangeable H^N sites of which 56 are backbone and two are N25 side chain/GlcNAc amide protons. Of the hydroxyl sites only T5 is observable (6.079 ppm) at the employed sample conditions. By comparison of the peak areas of the $^1H^C$ and $^1H^{N,O}$ signals of sample B, the average $^2H^C$ deuteration level was estimated to be >99%. This value fulfils expectations given a ^{2}H content of 99% in methanol-d_4 (Cambridge Isotope Labs) and 99.9% in D_2O (Isotec). Deuteration levels may be expected to be highest for H^α, which is taken exclusively from the solvent [27].

2.2. Measurement of $^1H^N$ longitudinal relaxation

As commented upon previously [28], for reasons of accuracy and time restraints $^1H^N$ longitudinal relaxation was monitored by one-dimensional inversion-recovery experiments. The pulse scheme proposed by Freeman and Hill [29], in which the $^1H^N$ longitudinal magnetisations $H_z(t)$ and $H_z(\infty)$ are acquired on alternate scans and subtracted so that the difference magnetisation is collected directly, was used. $^1H^N$ assignments of the 1D spectra were obtained from the known ^{2}F2 shifts [26] and their H–N HSQC correlations. As can be seen in the illustrative 1D ^{1}H spectrum, Fig. 1A, overlap and broad peaks from exchangeable side chain protons are rare and do not interfere with the majority of the backbone $^1H^N$ resonances.

Inversion-recovery experiments were performed at 5 °C and ^{1}H frequencies of 500 and 750 MHz. The solvent magnetisation was controlled by a Gaussian shaped pulse [30] of 2.0 ms duration. During the relaxation delays, radiation damping of the solvent was suppressed by application of weak gradient pulses [31]; chemical shift anisotropy (CSA)-dipolar cross-correlation effects

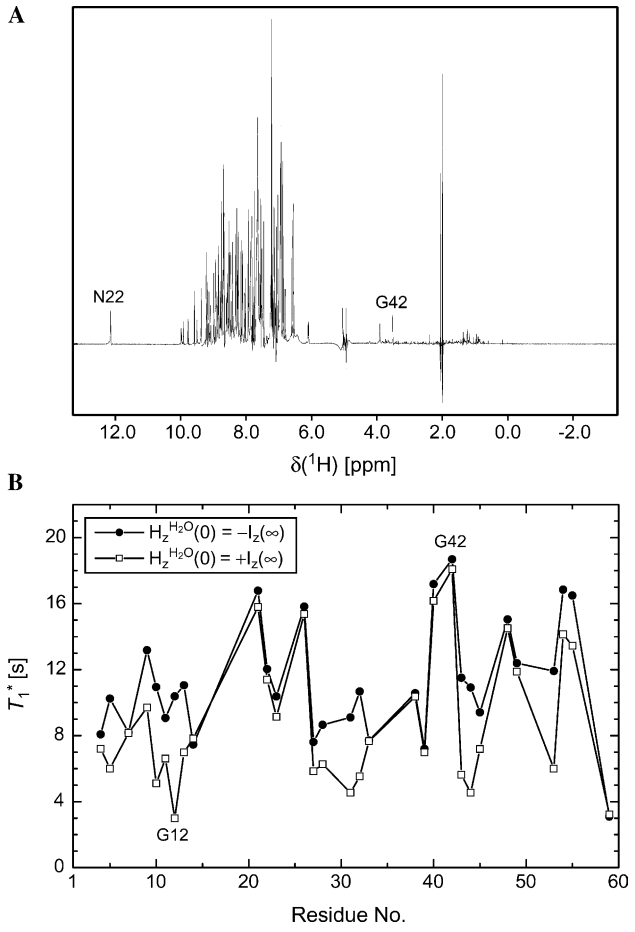

Fig. 1. (A) ^{1}H 1D spectrum of the 99% ^{2}H, 98% ^{15}N labelled second type 2 domain of fibronectin (^{2}F2) at a concentration of 2 mM in 90%/10% H_2O/D_2O solution, pH 4.0, at 5 °C and 750 MHz. Trace amounts of citrate and acetate are present. The chemical shift of the backbone amide protons ($^1H^N$) range from 3.490 (G42) to 12.177 ppm (N22). Thirty one out of 55 backbone $^1H^N$ resonances were resolved at 750 MHz. (B) T_1^* time constants for non-selective $^1H^N$ inversion-recoveries with initial solvent magnetisations of $+I_z(\infty)$ or $-I_z(\infty)$ as a function of residue number. Measurement errors are below 5%; error bars are omitted for clarity.

were removed by the application of 180° ^{15}N pulses every 80 ms [32,33]. Eight-thousand one-hundred ninety-two complex points were recorded during an acquisition time of 327.7 ms with ^{15}N decoupling using a GARP-1 profile [34] at 4.2 kHz. Recycle delays of 80 s (500 MHz) and 110 s (750 MHz) were used. For sample A, non-selective longitudinal relaxation recoveries at 500 MHz were sampled at 16 different time points, ranging from 0.16 to 14.4 s. At 750 MHz, data were recorded twice using the two independently prepared A samples. Seventeen different time points were recorded; in the first case, they ranged from 0.16 to 20.8 s and, in the second case, they ranged from 0.16 to 32.8 s. Within experimental errors, no difference between the two A samples was found for $^1H^N$ nuclei without significant solvent chemical exchange contributions (see Section 3.2). For sample B, longitudinal relaxation recoveries at 750 MHz were sampled at 5 different time points, ranging from 0.64 to 17.6 s. Selective inversion-recovery experiments were carried out at 750 MHz employing sample A. After inversion of a $^1H^N$ resonance by a rectangular pulse of 36.5 ms duration, 17 different time points, ranging from 0.16 to 32.8 s, were recorded.

Data were processed with Felix 2.3 (Biosym). Uncertainties in peak intensities were determined from duplicate data points. The measured recoveries were subjected to a two-parameter mono-exponential fit:

$$I(t) = I(0)\exp(-R_1^* t) \quad (1)$$

to extract an apparent rate constant, R_1^*. Monte Carlo simulations were performed to estimate errors.

2.3. Measurement of $^1H^N$ transverse relaxation

The 2D pulse sequence described by Ishima et al. [20] with $^1H^N$ relaxing as unlike spins was used. Experiments were carried out at 5 °C and 750 MHz with a recycle delay of 10 s. Matrices consisting of 2048 × 128 complex points were collected using acquisition times of 81.9 and 53.5 ms in the $^1H^N$ and ^{15}N dimension, respectively. Chemical shift anisotropy (CSA) and dipolar cross-correlation was removed by application of nitrogen 180° pulses in the middle of the basic CPMG block [35]. Eight relaxation delays ranging from 6.7 to 134.3 ms and a CPMG delay of 400 μs were used. During the CPMG period the B_1 field strength was reduced from 27.8 to 12.6 kHz and the ^{1}H transmitter frequency was shifted from 4.950 to 8.293 ppm. Uncertainties in peak intensity data were estimated from the spectral noise. The obtained recoveries were subjected to a two-parameter mono-exponential fit, Eq. (1), to extract an apparent rate constant, R_2^*.

2.4. Measurement of the decay of two-spin order $2H_zN_z$

The pulse sequence described by Skrynnikov et al. [36], which removes any influence from CSA-dipolar cross-correlation phenomena upon the measured decay rates, was used in a 1D fashion. With sample A, 14 relaxation delays ranging from 0.002 to 2 s were collected at 5 °C and 750 MHz. Uncertainties in peak intensities were determined from duplicate data points. The recoveries obtained were subjected to a two-parameter mono-exponential fit, Eq. (1), to extract an apparent rate constant, $(\mu + \sigma)^*$.

2.5. Calculation of $^1H^N$ proton relaxation rates

In the case of transverse relaxation it is, in general, straightforward to formulate the transverse relaxation rate, R_2^* of spin i as the sum of several distinct relaxation contributions [20]:

$$R_2^*({}^1H_i^N) = R_2({}^1H^N\text{–}{}^{15}N\ DD) + R_2({}^1H^N CSA) + n\sum_{i\neq j} R_2({}^1H_i^N\text{–}{}^1H_j^{N,O}\ DD) + m\sum_{i\neq j} R_2({}^1H_i^N\text{–}{}^1H_j^C\ DD) + (1-n)\sum_{i\neq j} R_2({}^1H_i^N\text{–}{}^2H_j^{N,O}\ DD), + (1-m)\sum_{i\neq j} R_2({}^1H_i^N\text{–}{}^2H_j^C\ DD), \quad (2)$$

where CSA denotes the relaxation rate due to chemical shielding anisotropy. DD denotes the rate due to dipole–dipole interactions. n and m denote weighting factors to account for the deuteration levels, $n\%/(1-n)\% = [H_2O/D_2O]$ and $m\%/(1-m)\% = [{}^1H^C/{}^2H^C]$. The longitudinal self- and cross-relaxation rates of spin I, ρ_I and σ_I, may be calculated in a similar manner:

$$\rho_I({}^1H^N) = \rho({}^1H^N CSA) + \rho({}^1H^N\text{–}{}^{15}N\ DD) + n\sum_{i\neq j} \rho({}^1H_i^N\text{–}{}^1H_j^{N,O}\ DD) + m\sum_{i\neq j} \rho({}^1H_i^N\text{–}{}^1H_j^C\ DD) + (1-n)\sum_{i\neq j} \rho({}^1H_i^N\text{–}{}^2H_j^{N,O}\ DD) + (1-m)\sum_{i\neq j} \rho({}^1H_i^N\text{–}{}^2H_j^C\ DD), \quad (3a)$$

$$\sigma_I({}^1H^N) = n\sum_{i\neq j} \sigma({}^1H_i^N\text{–}{}^1H_j^{N,O}\ DD) + m\sum_{i\neq j} \sigma({}^1H_i^N\text{–}{}^1H_j^C\ DD). \quad (3b)$$

As outlined in Section 1, the short ^2H self-relaxation rate renders cross-relaxation between ^1H–^2H nuclei negligible. The contribution to cross-relaxation from $\sigma({}^1H^N\text{–}{}^{15}N\ DD)$ is typically estimated to be <3% of the total cross-relaxation rate and is neglected in the following discussion. ^{2}F2 has 438 proton sites and, hence, the isotopically enriched sample is composed of many distinct isotopic ^{2}F2 configurations (isotopomers). Assuming all of these are stable over the timescale of the rate measurements they will relax independently of each other, but each $^1H^N$ contributes intensity to the same resonance. Therefore, averaging of $^1H^N$–^1H and $^1H^N$–^2H dipolar contributions using the weighting factors n and m, rather than considering the ensemble of different isotopomers, represents an approximation. Clearly the dipolar relaxation contributions from $^1H_i^{N}\text{–}^{1,\,2}H_j^{N,O}$ and $^1H_i^{N}\text{–}^{1,\,2}H_j^{C}$ interactions could exhibit distinct correlation functions with different time scales for internal motion.

The formulation of the longitudinal two-spin order self-relaxation rate, $\mu(H_zN_z)^*$, assuming no CSA-dipolar cross-correlation processes which can interconvert Zeeman single spin and longitudinal two spin order magnetisations, is:

$$\mu(H_zN_z)^* = \rho({}^1H^N\ CSA) + \rho({}^{15}N\ CSA) + \rho(H_{iz}N_{iz}\ DD) + n\sum_{i\neq j} \rho(H_{iz}N_{iz}\text{–}{}^1H_j^{N,O}\ DD) + m\sum_{i\neq j} \rho(H_{iz}N_{iz}\text{–}{}^1H_j^C\ DD) + (1-n)\sum_{i\neq j} \rho(H_{iz}N_{iz}\text{–}{}^2H_j^{N,O}\ DD) + (1-m)\sum_{i\neq j} \rho(H_{iz}N_{iz}\text{–}{}^2H_j^C\ DD). \quad (4a)$$

The cross-relaxation rate amongst the two-spin order terms is:

$$\sigma(H_zN_z) = n\sum_{i\neq j} \sigma(H_{iz}N_{iz}\text{–}{}^1H_j^{N,O}\ DD) + m\sum_{i\neq j} \sigma(H_{iz}N_{iz}\text{–}{}^1H_j^C\ DD), \quad (4b)$$

where contributions to the cross relaxation rate from dipole–dipole ($H_{iz}N_{iz}$–$H_{jz}N_{jz}$) cross-correlation processes have been ignored.

R^* rates were calculated using standard equations [21] employing the isotropic model-free correlation function [37]. A vibrationally averaged ^{15}N–H internuclear distance of 1.04 Å was used [38] and the H–H distances were derived from the average ^{2}F2 NMR structure [26]. An axially-symmetric ^{15}N CSA tensor with magnitude, $\Delta\sigma$, of −163 ppm [39–41] and a $^1H^N$ CSA tensor with $\Delta\sigma = 8.7$ ppm and $\eta = 1$ [40] were assumed.

3. Results and discussion

3.1. General considerations

Longitudinal relaxation in a system of i dipolar-coupled spins, with cross-correlation suppressed [32,33], is generally a multi-exponential process. Assuming no chemical exchange, it is governed by a set of coupled differential equations of the form [42]:

$$d[I_z^i(t) - I_z^i(\infty)]/dt = -\rho_i[I_z^i(t) - I_z^i(\infty)] - \sum_{i\neq j} \sigma_{ij}[I_z^j(t) - I_z^j(\infty)], \quad (5)$$

where $I_z^i(t)$ denotes the expectation value of the Zeeman operator, I_z, of spin i at time t, ρ_i denotes the self-relaxation rate of spin i and σ_{ij} denotes the pairwise cross-relaxation rate between spins i and j. The many different relaxation processes contributing to ρ in a ^{2}H, ^{15}N labelled protein are summarised in Table 1. In the following we report a simple phenomenological description of the recoveries of $^1H^N$ longitudinal magnetisation where the experimental recovery curves are subjected to a two-parameter mono-exponential fit, Eq. (1), to extract an apparent rate constant, R_1^* (Fig. 2A). This definition for R_1^* represents a special case of Eq. (5) and

Table 1
Relaxation processes contributing to the $^1H^N$ longitudinal self-relaxation rate, ρ, in a ^2H, ^{15}N-labelled protein

Contribution[a]
I. $^1H^N$ chemical shielding anisotropy (CSA)
II. $^1H^N$–^{15}N dipole–dipole (DD) interaction
III. $^1H^N$–$^1H^{N,O,C}$ DD interactions
IV. $^1H^N$–$^2H^{N,O,C}$ DD interactions
V. $^1H^N \leftrightarrow H_2O$ chemical exchange
VI. $^1H^N$ paramagnetic relaxation

[a] Contributions I and II are referred to as *local*, III and IV as *remote* and V and VI as *external*.

occurs whenever, for a two-spin system, I–S, the self-relaxation rate constants, ρ_I and ρ_S, and their gyromagnetic ratios are identical. In this situation, the time dependence of the longitudinal magnetisation of spin I (or S) following non-selective inversion is

$$[I_z(t) - I_z(\infty)]/[I_z(0) - I_z(\infty)] = \exp -(\rho + \sigma)t, \qquad (6)$$

and the recovery exhibits a (mono-exponential) longitudinal relaxation rate, R_1 equal to $\rho + \sigma$. Consider the general situation of a proton spin i surrounded by j proton spins where the surrounding protons are increasingly diluted by deuterons. Statistically it follows that, for a large majority of molecules, either the proton spin i will be surrounded only by deuterons or have only one other proton in the vicinity; this spin-pair can be considered to be effectively isolated. In this situation *spin diffusion* will be negligible, as there will be very few proton relay partners left beyond the isolated H–H pair. Therefore, in the limit of high sample deuteration it becomes a good approximation to consider the environment of a $^1H^N$ nucleus as primarily composed of many distinct pairwise H–D interactions and isolated pairwise H–H interactions. The observable longitudinal relaxation rate may also be described as the weighted sum of the pairwise H–D and H–H interactions, for all isotopomers, as indicated by Eq. (3a) and (3b). For a proton spin pair in this highly deuterated milieu the ^1H–^1H dipolar interactions will dominate both ρ and σ, and the assumptions of identical self-relaxation constants and the application of Eq. (6) with $R_1^* = \sigma_I + \rho_I$ are expected to be acceptable approximations.

What are the expected magnitudes of the various relaxation contributions, highlighted in Table 1, that contribute to R_1^*? Some simple model calculations have been carried out, assuming restricted internal H–N motion, overall isotropic rotational diffusion and the following parameters, $B_0 = 17.6\,T$, $\tau_r = 8.5\,ns$, $S^2 = 0.96$, $\tau_i = 143\,ps$, $n = 10\%$ and $m = 1\%$, in addition to those described in Section 2.5. Only four spin pairs, $^1H^N$–$^1H^{N,O}$, $^1H^N$–$^1H^C$, $^1H^N$–$^2H^{N,O}$ and $^1H^N$–$^2H^C$, are assumed to contribute to Eqs. (3a) and (3b) and their internuclear distances specifically characterise the local environment of the $^1H^N$ nucleus I. Assuming values for d(H^N–$H^{N,O}$) of 2.42 Å and d(H^N–H^C) of 1.82 Å

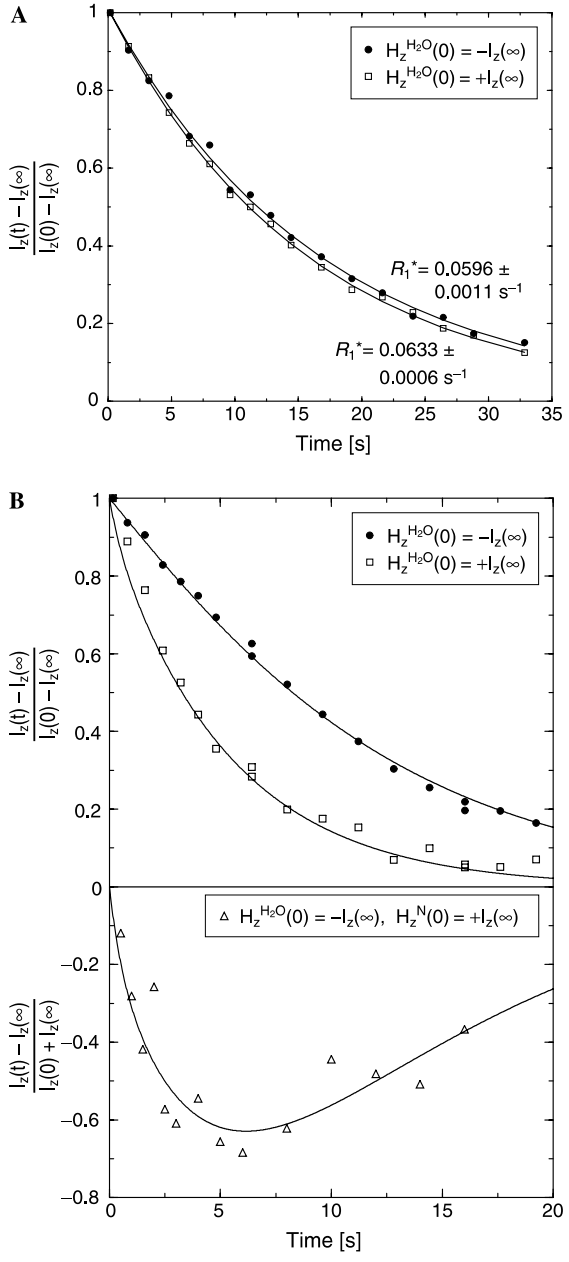

Fig. 2. Examples of non-selective $^1H^N$ inversion-recovery experiments where either the initial solvent magnetisation, $H_z^{H_2O}$ (0), was equal to $+H_z^{H_2O}$ (∞) or $-H_z^{H_2O}$ (∞) or the solvent was selectively inverted with the $^1H^N$ magnetisations remaining at their equilibrium values of $+I_z$ (∞). The experiments were carried out at 5 °C and 750 MHz in a degassed 10%/90% H_2O/D_2O solution, pH 4.0, employing the 99% ^2H, 98% ^{15}N labelled second type 2 domain of fibronectin ($^2F2$) at a concentration of 2 mM. The behaviour of the $^1H^N$ nucleus of (A) Y21 and (B) S10, respectively, are shown. (A) For Y21 no changes to the $^1H^N$ magnetisation are detected upon selective inversion of the solvent. The rate constants extracted from mono-exponential fits, Eq. (1), to each dataset, having initial solvent magnetisations of $+H_z^{H_2O}$ (∞) and $-H_z^{H_2O}$ (∞), respectively, differ by only $0.004\,s^{-1}$. (B) In contrast, for S10 solvent magnetisation can be readily transferred to the $^1H^N$ nucleus. Simulated fits to these data are shown using a two-spin model having identical self-relaxation rates, ρ, of $0.973\,s^{-1}$, a cross-relaxation rate, σ, of $-0.934\,s^{-1}$ and an apparent first-order solvent exchange rate, k_{ex}^* of $0.25\,s^{-1}$. The experimentally determined self-relaxtion time constant of the solvent was 8.9 s [28].

(equivalent to four deuterons each at 2.3 Å) we obtain for $\rho + \sigma$ 0.0598 s^{-1}. In this case the local contributions represented by the $^1H^N$ CSA (0.0027 s^{-1}) and $^1H^N$–^{15}N dipolar interactions (0.045 s^{-1}) are about 80% of the total longitudinal R_1^* rate. The next most important contribution, 13%, is calculated to be from the dipolar interactions involving the carbon bonded deuteron spins $^1H^N$–$^2H^C$ (0.0080 s^{-1}) with the other dipolar processes involving $^1H^N$–$^1H^{N,O}$, $^1H^N$–$^1H^C$, and $^1H^N$–$^2H^{N,O}$ interactions providing the remainder. The transverse R_2^* rate is calculated to be 12.7 s^{-1}, Eq. (2), which is in good agreement with the average experimental value of 12.5 ± 1.5 s^{-1} for a $^1H^N$ site in a regular secondary structure element of ^{2}F2. The relative contributions to R_2^* from the remote interactions as well as the ratio of local to remote processes are predicted to be of quite similar proportions to those calculated for R_1^*. However, the relative contributions of the two local processes, $^1H^N$ CSA and $^1H^N$–^{15}N dipolar, do change. The $^1H^N$ CSA contribution to the total rate is 12.8% for R_2^* and only 4.5% for R_1^*, whereas for $^1H^N$–^{15}N dipolar interactions the corresponding values are 64.8% and 75.0%, respectively. The rate constant, $\mu + \sigma$, for the longitudinal two-spin order, is predicted to be quite large, approximately 19-times larger than $\rho + \sigma$, due to significant contributions from the local processes ρ (^{15}N CSA) and ρ ($H_{iz}N_{iz}$ DD).

Lowering the solvent ratio from 10 to 1% H_2O is predicted to reduce R_2^* by only 4% and the longitudinal relaxation rate, R_1^* is predicted to reduce by about 1%. These values are inside the experimental uncertainties. In the limit that the solvent H_2O content tends toward zero, the maximum $^1H^N$ longitudinal relaxation time, $T_1^* = 1/R_1^*$ is predicted, using these parameters, to be 17.2 s. The rate constant R_1^* is expected to show a pronounced frequency dependence and at $B_0 = 11.6$ T, is predicted to increase to 0.105 s^{-1} whereas R_2^* changes by less than 2%. Moreover, as illustrated in Fig. 3, both R_1^* and R_2^* are sensitive to the amplitude of the internal motion, $\boldsymbol{S}^2$, but only R_1^* is sensitive to the timescale of the internal motion, τ_i.

For the 99% ^2H, 98% ^{15}N-labelled ^{2}F2 sample in degassed 10%/90% H_2O/D_2O, a wide distribution of T_1^* values is obtained, ranging from 3.0 to 18.7 s (Fig. 1B). This wide range implies that spin diffusion has been significantly diminished by the high dilution of ^1H spins. Moreover, depending on the spin state of the solvent, large differences in the T_1^* time constants were observed for the majority of $^1H^N$ nuclei (Fig. 1B). Paramagnetic contributions from dissolved atmospheric oxygen represent significant and highly inhomogeneous contributions to the slow $^1H^N$ longitudinal relaxation rates [28,43]. The use of degassed sample solutions is therefore mandatory.

3.2. Influence of solvent magnetisation

Solvent magnetisation may be transferred to $^1H^N$ nuclei either by direct chemical exchange, $H_2O \rightarrow {}^1H^N$,

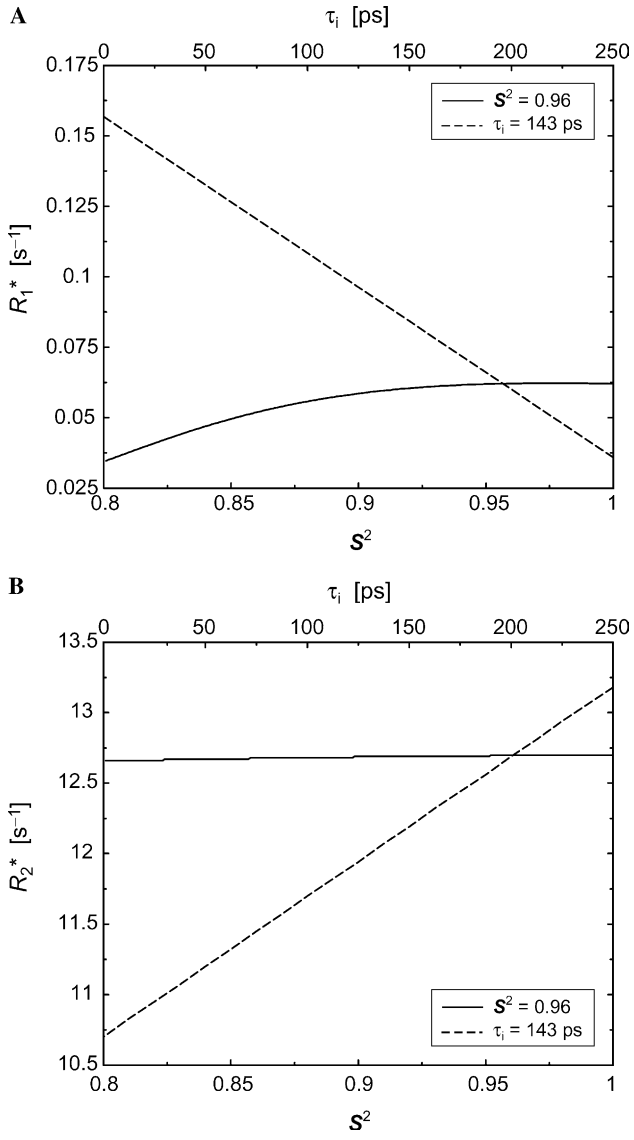

Fig. 3. Calculated dependence of the R_1^* and R_2^* $^1H^N$ relaxation rates on the model-free parameters $\boldsymbol{S}^2$ and τ_i at a field strength of 17.6 T. The calculated values for R_1^* and R_2^* were determined using Eqs. (2), (3a), and (3b) and employed the parameters described in Section 3.1. The calculations have been carried out using either a fixed $\boldsymbol{S}^2$ value and varying τ_i (solid line) or by varying $\boldsymbol{S}^2$ with a fixed τ_i value (dashed line).

or by cross-relaxation with nearby fast-exchanging protons, e.g., $H_2O \rightarrow {}^1H^O \cdots {}^1H^N$ [44]. If the reverse process, which can lead to appreciable broadening of the solvent signal [45], is neglected, the solvent magnetisation is described by

$$d[H_z^{H_2O}(t) - H_z^{H_2O}(\infty)]/dt = -\rho^{H_2O}[H_z^{H_2O}(t) - H_z^{H_2O}(\infty)], \quad (7a)$$

which integrates to

$$H_z^{H_2O}(t) = [H_z^{H_2O}(0) - H_z^{H_2O}(\infty)] \exp -\rho^{H_2O} t + H_z^{H_2O}(\infty), \quad (7b)$$

where ρ^{H_2O} denotes the longitudinal relaxation rate of the bulk solvent. Introducing the solvent exchange process into the Solomon equations, Eq. (5), gives:

$$\begin{aligned} d[I_z^i(t) - I_z^i(\infty)]/dt = &-\rho_i[I_z^i(t) - I_z^i(\infty)] \\ &- \sum_{j\neq i} \sigma_{ij}[I_z^j(t) - I_z^j(\infty)] \\ &- k_{ex} I_z^i(t) + k_{ex} H_z^{H_2O}(t), \end{aligned} \quad (8)$$

where k_{ex} denotes the apparent pseudo-first order exchange rate of spin i with the solvent. Combining Eqs. (7b) and (8) gives

$$\begin{aligned} d[I_z^i(t) - I_z^i(\infty)]/dt = &-(\rho_i + k_{ex})[I_z^i(t) - I_z^i(\infty)] \\ &- \sum_{j\neq i} \sigma_{ij}[I_z^j(t) - I_z^j(\infty)] \\ &+ k_{ex}[H_z^{H_2O}(0) - H_z^{H_2O}(\infty)] \\ &\times \exp -\rho^{H_2O} t, \end{aligned} \quad (9)$$

implying that, for non-selective T_1 experiments, the longitudinal relaxation of the $^1H^N$ nuclei is coupled to the longitudinal relaxation characteristics of the solvent, ρ^{H_2O}, whenever there is chemical exchange in analogy to cross-relaxation among the protein ^1H spins themselves.

The effect of solvent exchange is illustrated by the behaviour of the $^1H^N$ nucleus of S10, which exhibits pronounced effects (Fig. 2B). An apparent exchange rate, k_{ex}^* can be estimated from the difference of the initial relaxation conditions and a knowledge of ρ^{H_2O}, as shown in Fig. 2B, yielding $0.25\,s^{-1}$ for S10. Sequence based predictions of the intrinsic $^1H^N \leftrightarrow H_2O$ exchange rates [46] give an average rate of $0.0081 \pm 0.0088\,s^{-1}$ at pH 4.0 and 5 °C. This relatively low average value suggests that the backbone amides can be significantly coupled to the solvent through cross-relaxation with fast exchanging side-chain protons, which immediately adopt the magnetisation state of the solvent.

As chemical exchange adds another non-linear complication to the /description of longitudinal relaxation, we prefer to exclude all $^1H^N$ nuclei exhibiting significant exchange phenomena from further analysis. Exchange is considered to be insignificant, if the difference between R_1^* rates measured at initial solvent magnetisations of $+H_z^{H_2O}$ (∞) and $-H_z^{H_2O}$ (∞), respectively, is smaller than $0.01\ s^{-1}$ and if no magnetisation can be transferred to the $^1H^N$ nucleus upon selective inversion of the solvent magnetisation (corresponding to the situation shown in Fig. 2A). This leaves 11 out of the 31 experimental $^1H^N$ longitudinal relaxation rates.

3.3. Correlation of $^1H^N$ relaxation rates with structural environment

Within the assumptions outlined in Section 3.1, the experimental relaxation rates, R_1^* and R_2^* of the $^1H^N$ nuclei may correlate with their respective $^1H/^2H$ structural environments. Assuming a rigid structure the distance parameter,

$$r_{IS}^{-6} = \sum_{i\neq j} r^{-6}(H_i^N, H_j), \quad (10)$$

conveniently defines the $^1H/^2H$ structural environment of a protein $^1H^N$ spin. Employing the ^{2}F2 average static NMR structure [26], values of $r_{IS}^{-6\,N,O}$ and $r_{IS}^{-6\,C}$, defining the H_i^N–$H_j^{N,O}$ and H_i^N–H_j^C environment of spin i, were calculated for the eleven $^1H^N$ nuclei with no significant solvent exchange. For these nuclei the distances $r_{IS}^{-6\,N,O}$ and $r_{IS}^{-6\,C}$ are found to range between 0.00056 and $0.0266\,Å^{-6}$ and 0.0116–0.0341 $Å^{-6}$, respectively, and the variation to $r_{IS}^{-6\,C}$ is smaller. Employing identical parameters to those in Section 3.1 the $^1H^N$–$^{1/2}H^{N,O}$ dipolar processes are predicted to contribute up to 25% to R_1^* and also up to 25% to R_2^*. A correlation between the defined $^1H^N$ relaxation rates and the structural environment, in particular with neighbouring $H^{N,O}$ sites, is, thus, to be expected.

A very good correlation is found between the experimental R_1^* relaxation rates and the parameter $r_{IS}^{-6\,N,O}$ (Fig. 4A). Excluding the two outliers, L14 and N22, the squared correlation coefficient for the 750 MHz, 10% H_2O dataset consisting of nine experimental measurements is $R^2 = 0.988$. The chemical shift of the $^1H^N$ nucleus of N22 is at 12.177 ppm (Fig. 1A) suggesting an interaction with the nearby $^-$OOC group of D48. At pH 4.0 a small fraction of HOOC may also be present, which could explain the observed deviation from $r_{IS}^{-6\,N,O}$, which is calculated for the deprotonated state only. For L14 the ^{2}F2 NMR structure shows the $^1H^N$ nucleus to be solvent exposed [26], although no solvent exchange was detected, thus a long-lived $^1H^N$–HOD interaction may perhaps explain the accelerated rate. The $R_1^* - r_{IS}^{-6\,C}$ correlation is found to be weaker, $R^2 = 0.690$, and it is noted that, for this subset of residues, the $^1H^N$ sites having a high $r_{IS}^{-6\,N,O}$ value exhibit a relatively low $r_{IS}^{-6\,C}$ value (Supplementary Fig. 1A and Fig. 4A). The squared correlation coefficient between R_2^* and $r_{IS}^{-6\,N,O}$, excluding N22 and W40, $R^2 = 0.47$, is significantly lower than that found between $R_1^* - r_{IS}^{-6\,N,O}$ (Fig. 4B). Measurement of R_2^* with different CPMG delays (data not shown), revealed that both D22 and W40 have conformational exchange contributions. The correlation between R_2^* and $r_{IS}^{-6\,C}$ is weaker than that between R_2^* and $r_{IS}^{-6\,N,O}$ (Supplementary Fig. 1B).

A less good correlation between R_2^* and $r_{IS}^{-6\,N,O}$ than obtained for R_1^* is unexpected. Based upon the relatively few measurements available from this sample it is, unfortunately, not possible to provide a clear explanation for this difference. As discussed in Section 3.1, the relative contributions from $^1H^N$ CSA relaxation processes are expected to be larger for the R_2^* rates than for the R_1^* rates. Thus, site-specific $^1H^N$ CSA variations [47] could contribute to the observed difference in correlation.

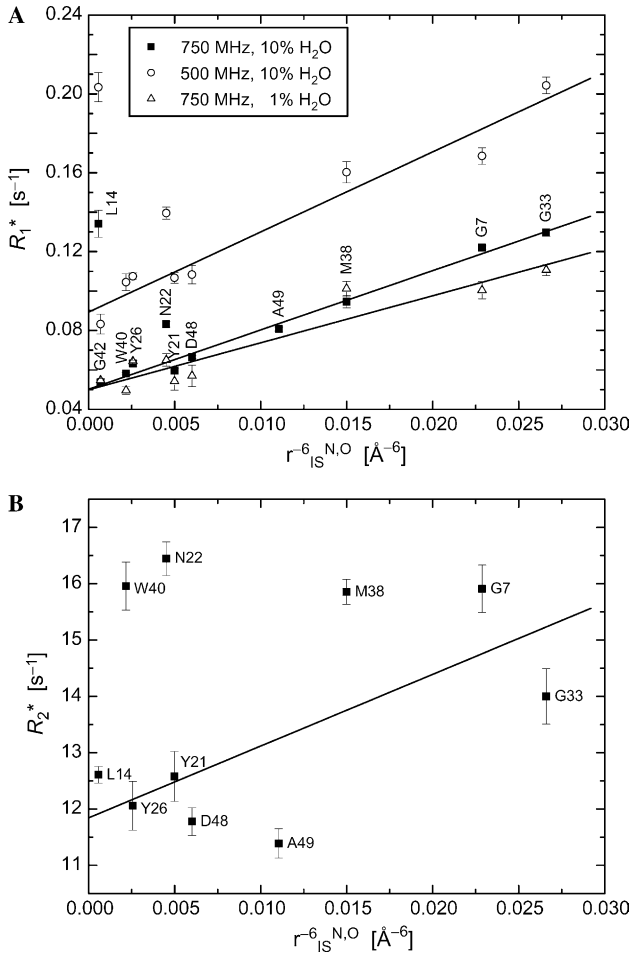

Fig. 4. (A) Correlation of R_1^* rates for $^1H^N$ nuclei without significant solvent chemical exchange with their $^{1/2}H^{N,O}$ structural environment, $r_{IS}^{-6\,N,O}$. R_1^* rates were measured at 750 MHz in degassed 1%/99% and 10%/90% H_2O/D_2O solutions, and at 500 MHz in degassed 10%/90% H_2O/D_2O solution. In all cases the initial solvent magnetisation $H_z^{H_2O}(0)$ was set to $-H_z^{H_2O}$ (∞). $r_{IS}^{-6\,N,O}$ values were calculated from the coordinates of the average ^{2}F2 NMR structure [26]. At 500 MHz, R_1^* of A49 could not be extracted due to spectral overlap. Compared to the dataset recorded in 10%/90% H_2O/D_2O, the 1%/99% H_2O/D_2O data were processed with a relatively weak window function, resulting in increased spectral overlap, which hampered the extraction of R_1^* rates for L14 and A49. Linear fits to the data are shown, whereby the two apparent outliers, L14 and N22, are excluded. At 500 MHz, 10% H_2O, $R_1^* = 4.06\,\text{Å}^6\,s^{-1}\ r_{IS}^{-6\,N,O} + 0.0893\,s^{-1}$ with a correlation coefficient, R, of 0.977. At 750 MHz, 10% H_2O $R_1^* = 3.01\ \text{Å}^6\,s^{-1}\ r_{IS}^{-6\,N,O} + 0.0502\,s^{-1}$ and $R = 0.994$. At 750 MHz, 1% H_2O, $R_1 = 2.38\,\text{Å}^6\,s^{-1}\ r_{IS}^{-6\,N,O} + 0.0499\,s^{-1}$ and $R = 0.945$. (B) Correlation of the transverse relaxation rates, R_2^* with the $^{1/2}H^{N,O}$ structural environment, $r_{IS}^{-6\,N,O}$, of the $^1H^N$ nuclei shown in (A). R_2^* rates were measured at 750 MHz in 10%/90% H_2O/D_2O solution. A linear fit to the data is shown, whereby N22 and W40 are excluded. Comparison of R_2^* rates at different CPMG delays indicates that N22 and W40 undergo conformational exchange (data not shown). $R_2^* = 127.4\text{Å}^6\ s^{-1}\ r_{IS}^{-6\,N,O} + 11.84\ s^{-1}$ and $R = 0.682$.

As shown in Fig. 3, the simulations also indicate that R_1^* is quite sensitive to the timescale of any internal motions in contrast to R_2^* Residues on the left hand side of Fig. 4 have a tendency to be in the domain core, whereas the residues on the right side tend to be closer to the surface. It is also possible that a correlation between the $r_{IS}^{-6\,N,O}$ parameter and the dynamic environment exists. In light of this, dynamic effects alone may also explain the faster relaxation rate of L14, which is located on the protein surface. A final remark is made about the maybe surprisingly high apparent quality of the $R_1^* - r_{IS}^{-6\,N,O}$ correlation. A weak anti-correlation between $r_{IS}^{-6\,N,O}$ and $r_{IS}^{-6\,C}$ (Fig. 4 and Supplementary Fig. 1) may contribute to this behaviour and indeed there may also possibly be some influence from the fact that the $^1H^N$–$^1H^N$ NOEs were used in the NMR structure calculation.

Fig. 4A permits a number of interesting conclusions to be drawn. For those $^1H^N$ nuclei with low $r_{IS}^{-6\,N,O}$ distance values identical experimental R_1^* rates are found, within the measurement errors, when employing solvent compositions containing either 1 or 10% H_2O. The following conclusions can be made for these $^1H^N$ sites. First, differences attributable to ensemble averaging of R_1^* rates from different ^{2}F2 isotopomers in 1 and 10% H_2O are not discernible. Second, spin diffusion must be extremely small and lastly the differences between the individual self-relaxation rates, ρ_i, must also be fairly small as many more $^1H^N$–^1H spin pairs exist in 10 than in 1% H_2O. In this context, it is also interesting to note that the R_1^* rates vary 2.4-fold in contrast to the R_2^* rates which only vary by a factor of 1.4 (Fig. 4). Again motion may contribute to the increased spread of R_1^* values (Fig. 3). As remarked above, the relative contributions of remote relaxation processes to R_1^* and to R_2^* are not predicted to be substantially different within the assumption of identical self-relation rates for ^1H–^1H spin pairs. Small imbalances in self-relaxation rates, only conceivable for residues with high $r_{IS}^{-6\,N,O}$ values (Fig. 4A), would change the sensitivity of R_1^* to remote relaxation processes, though, and also contribute to an increased spread in R_1^* rates.

3.4. $^1H^N$ relaxation rate calculations, selective inversion recovery and decay of longitudinal two-spin order

For six out of the eleven residues without significant solvent chemical exchange accurate $^1H^N$ relaxation measurements were obtained for the R_1^* (10% H_2O, 500 MHz), R_1^* (10% H_2O, 750 MHz), R_1 (1% H_2O, 750 MHz), and R_2^* (10% H_2O, 750 MHz) rates (Fig. 4). Fitting of the rates using two model-free parameters, $\boldsymbol{S}^2$ and τ_i [37], yielded a statistically satisfactory description of the experimental measurements for four out of the six residues (Table 2). As discussed in the previous section, for residues Y21 and Y26 the assumption of identical self-relaxation rates underlying the calculation of R_1^* has been experimentally validated (Fig. 4A). For G7 and M38 relatively slow R_2^* rates (Fig. 4B) were the primary cause of the slightly poorer fits to the experimental data (Supplementary Table 1). Measurement of their R_2^* rates with different CPMG delays did not show any

Table 2
Parameterisation of model-free correlation function that minimise the difference between experimental and predicted R_1^* (10% H_2O, 500 MHz), R_1^* (10% H_2O, 750 MHz), R_1 (1% H_2O, 750 MHz), R_2^* (10% H_2O, 750 MHz) rates and comparison with values obtained from ^{15}N relaxation analysis[a]

Residue[b]	S^2 [$^1H^N$][c]	τ_i [$^1H^N$]/ps	χ_n^2 [$^1H^N$][d]	S^2 [^{15}N]	τ_i [^{15}N] /ps[e]
Y26	0.94 ± 0.02	114 ± 30	0.64	0.92 ± 0.02	70 ± 52
Y21	0.96 ± 0.02	143 ± 66	0.28	0.97 ± 0.02	—
D48	0.88 ± 0.01	46 ± 70	0.64	1.00 ± 0.01	<10
M38	0.92 ± 0.02	233 ± 133	40.1	0.91 ± 0.01	122 ± 43
G7	0.86 ± 0.02	111 ± 20	14.9	1.00 ± 0.01	<10
G33	0.88 ± 0.04	194 ± 94	0.27	1.00 ± 0.01	<10

[a] Experimental and predicted $^1H^N$ rates are given in Supplementary Table 1. From the viscosities of H_2O and D_2O at 5 °C of 1.519 and 1.988 mPa s, respectively [48] a 1.022-fold higher τ_c was assumed in 1%/99% H_2O/D_2O than in 10%/90% H_2O/D_2O. The ^{15}N relaxation rates, recorded at 25 °C and in 90%/10% H_2O/D_2O, are from reference [49] and were analysed analogously to the $^1H^N$ relaxation data employing an isotropic model [37] with the programme Modelfree 4.15 [55,56].

[b] An isotropic rotational correlation time, τ_c, of 8.5 ns was found in 10%/90% H_2O/D_2O.

[c] Monte Carlo simulations (500) were carried out to estimate uncertainties.

[d] Denotes the normalised χ^2 with $\chi_n^2 = \chi^2/(n-1)$, where n is the number of experimental restraints.

[e] For Y21 the Monte Carlo simulations showed that the ^{15}N data at hand do not restrict τ_i in a statistically significant manner.

conformational exchange contributions and local variations of $^1H^N$ CSA tensors could possibly be a contribution to the poor fits. Based on the viscosities of H_2O and D_2O and their temperature dependence [48], an isotropic rotational correlation time, τ_c, of 7.5 ns is predicted from the earlier ^{15}N relaxation studies of $^2F2$ (performed at 25 °C and 90%/10% H_2O/D_2O [49]). The larger τ_c in this case (8.5 ns) can be explained by a small amount of sample aggregation induced by the lower temperature and higher protein concentration compared to the ^{15}N study. The order parameter, S^2, obtained from the $^1H^N$ and ^{15}N datasets agree very well for three residues Y21, Y26, and M38 (Table 2) with the agreement being slightly less good for residues G7, G33, and D48 although the ^{15}N and $^1H^N$ derived S^2 values are within 15%.

Two additional experimental datasets—selective inversion profiles and the decay of longitudinal two-spin order—were also recorded (Fig. 5). The time dependence of a $^1H^N$ spin after selective inversion of its magnetisation in the case of a two-spin system exhibiting identical self-relaxation rate constants, ρ, and gyromagnetic ratios gives rise to a bi-exponential recovery according to:

$$[I_z(t) - I_z(\infty)]/[I_z(0) - I_z(\infty)] = 0.5[\exp -(\rho - \sigma)t + \exp -(\rho + \sigma)t], \quad (11)$$

where ρ and σ are given by Eqs. (3a) and (3b), respectively. Expressing the ^1H–^1H terms of Eq. (3a) and (3b) in terms of linear combinations of interlevel spin transition rates, p, for a two spin system gives [42]:

$$\rho^{HH} + \sigma^{HH} = (pZQ^{HH} + 2pSQ^{H} + pDQ^{HH}) + (pDQ^{HH} - pZQ^{HH}) = 2(pSQ^{H} + pDQ^{HH}) = R_1^{HH}, \quad (12a)$$

$$\rho^{HH} - \sigma^{HH} = 2(pZQ^{HH} + pSQ^{H}), \quad (12b)$$

with zero-quantum (ZQ) and double-quantum (DQ) spin transitions taking place between the two ^1H spins and single quantum (SQ) spin transition rates assumed to be identical for each ^1H spin. ZQ processes are quite abundant and the rate constant $\rho - \sigma$ will have a large contribution from dipole–dipole interactions involving $^1H_i^N$–$^1H_j^{N,O}$ and $^1H_i^N$–$^1H_j^C$ spins. It is these processes which accelerate the initial rate of recovery in comparison to non-selective recoveries. Imposing these initial conditions causes the longitudinal recovery to show pronounced non-exponential behaviour. The $^1H^N$ from Y21 clearly illustrates this type of behaviour, Fig. 5A. The relatively rapid decay of the longitudinal two-spin order, Fig. 5B, compared to that observed for the single spin magnetisation, H_z, is primarily due to contributions from local ^{15}N CSA and $H_{iz}N_{iz}$ intramolecular dipolar processes [50].

In order to successfully include the experimental restraints of Fig. 5 requires a more elaborate theoretical approach than presented here. The H^N–H^N and H^N–$H^{O,C}$ remote relaxation processes are characterised by segmental backbone motions and backboneside–chain torsion angle fluctuations and probably experience different internal dynamics associated with larger amplitude motions compared to those typically experienced by polypeptide backbone H–N atoms. In the analysis up to now we have assumed a rigid static protein, however, interresidue motions will not only reflect the dynamics of both residues but the average distance could also change.

4. Concluding Remarks

It has been shown that for a $^1H^N$ site in a highly deuterated protein a large array of $^1H^N$ relaxation parameters reflecting site-specific structural and dynamic information rather than averaged characteristics can be obtained. The relatively low contribution from the ^1H–^1H dipolar interactions in non-selective longitudinal inversion-recovery experiments makes a semi-quantita-

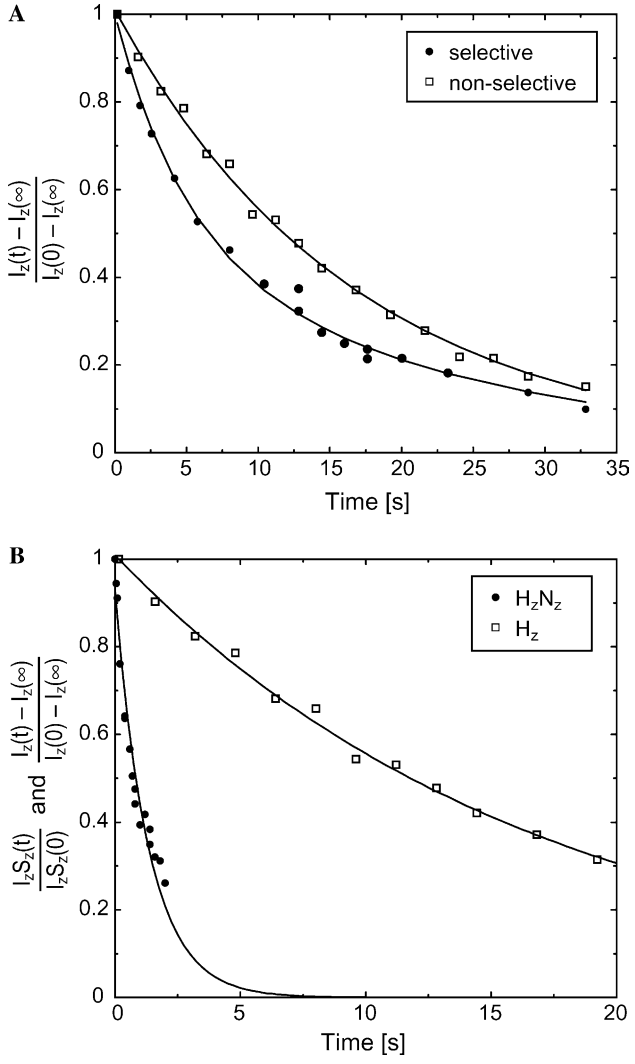

Fig. 5. (A) A comparison of the selective and non-selective $^1H^N$ inversion-recovery data for Y21. The experiments were conducted at 750 MHz in degassed 10%/90% H_2O/D_2O solution, pH 4.0. For the non-selective dataset the solid line represents the simulated recovery generated using the parameters shown in Table 2. The solid line through the selective dataset are an aid to visualisation only and represent the best fit using Eq. (11). (B) A comparison of the recovery of Y21 single-spin, H_z, and the decay of two-spin, $2H_zN_z$, magnetisations each recorded using non-selective initial conditions. The data were conducted at 750 MHz using a degassed 10%/90% H_2O/D_2O solution, pH 4.0 and illustrate the slow relaxation rate of the single-spin compared to the two-spin magnetisation.

tive interpretation of these data possible when assuming identical self-relaxation constants for isolated proton spin-pairs. A rigorous characterisation of the dynamic processes will require a more elaborate approach—an integration with molecular dynamics simulations appears desirable [51–53]—so that motional effects upon interresidue interactions can be estimated and the full use of selective inversion-recovery and the decay of two-spin order can be made. Although the data presented here were recorded in a 1D fashion, partly due to time constraints, non-selective inversion-recovery experiments with long interscan times may be amenable to 2D acquisition by employing only a few suitably chosen relaxation delays [54] thus allowing much greater sampling of the $^1H^N$ sites and leading to the study of larger proteins.

Acknowledgments

We are indebted to Andy Pickford for the ^{2}F2 deuteration protocol and substantial help during protein production. The help of Ulrich Schwarz-Linek during protein purification is also appreciated. We thank Ad Bax for critically reading the manuscript. TSU is supported by a Long-Term Fellowship from the Human Frontier Science Program. Financial support by the BBSRC and Wellcome is appreciated.

References

[1] E.Z. Eisenmesser, D.A. Bosco, M. Akke, D. Kern, Enzyme dynamics during catalysis, Science 295 (2002) 1520–1523.
[2] J.J. Chou, S.P. Li, C.B. Klee, A. Bax, Solution structure of Ca2+-calmodulin reveals flexible hand-like properties of its domains, Nat. Struct. Biol. 8 (2001) 990–997.
[3] A.J. Wand, Dynamic activation of protein function: a view emerging from NMR spectroscopy, Nat. Struct. Biol. 8 (2001) 926–931.
[4] A.G. Palmer, C.D. Kroenke, J.P. Loria, Nuclear magnetic resonance methods for quantifying microsecond-to-millisecond motions in biological macromolecules, Methods Enzymol. 339 (2001) 204–238.
[5] R. Ishima, D.A. Torchia, Protein dynamics from NMR, Nat. Struct. Biol. 7 (2000) 740–743.
[6] L.E. Kay, Protein dynamics from NMR, Nat. Struct. Biol. 5 (1998) 513–517.
[7] L.E. Kay, D.A. Torchia, A. Bax, Backbone dynamics of proteins as studied by N-15 inverse detected heteronuclear nmr-spectroscopy—application to staphylococcal nuclease, Biochemistry 28 (1989) 8972–8979.
[8] A. Kalk, H.J.C. Berendsen, Proton magnetic relaxation and spin diffusion in proteins, J. Magn. Reson. 24 (1976) 343–366.
[9] O. Millet, D.R. Muhandiram, N.R. Skrynnikov, L.E. Kay, Deuterium spin probes of side-chain dynamics in proteins. 1. Measurement of five relaxation rates per deuteron in C-13–labeled and fractionally H-2-enriched proteins in solution, J. Am. Chem. Soc. 124 (2002) 6439–6448.
[10] N.R. Skrynnikov, O. Millet, L.E. Kay, Deuterium spin probes of side-chain dynamics in proteins. 2. Spectral density mapping and identification of nanosecond time-scale side-chain motions, J. Am. Chem. Soc. 124 (2002) 6449–6460.
[11] H.L. Crespi, R.M. Rosenberg, J.J. Katz, Proton magnetic resonance of proteins fully deuterated except for 1 H-Leucine side chains, Science 161 (1968) 795–796.
[12] J.L. Markley, I. Putter, O. Jardetzky, High-resolution nuclear magnetic resonance spectra of selectively deuterated staphylococcal nuclease, Science 161 (1968) 1249–1251.
[13] C.K. Brush, M.P. Stone, T.M. Harris, Utilization of selective deuteration in Nmr spectral assignment of deoxyoligonucleotides—2d noesy analysis of non-self—complementary duplexes, Biochemistry 26 (1987) 4164–4164.

[14] M.K. Rosen, K.H. Gardner, R.C. Willis, W.E. Parris, T. Pawson, L.E. Kay, Selective methyl group protonation of perdeuterated proteins, J. Mol. Biol. 263 (1996) 627–636.
[15] A. Zvi, D.J. Feigelson, Y. Hayek, J. Anglister, Conformation of the principal neutralizing determinant of human immunodeficiency virus type 1 in complex with an anti-gp120 virus neutralizing antibody studied by two-dimensional nuclear magnetic resonance difference spectroscopy, Biochemistry 36 (1997) 8619–8627.
[16] J.D. Gross, V.M. Gelev, G. Wagner, A sensitive and robust method for obtaining intermolecular NOEs between side chains in large protein complexes, J. Biomol. NMR 25 (2003) 235–242.
[17] T. Yamazaki, W. Lee, M. Revington, D.L. Mattiello, F.W. Dahlquist, C.H. Arrowsmith, L.E. Kay, An HNCA pulse scheme for the backbone assignment of N-15,C-13,H-2-labeled proteins—application to a 37-kDa TRP Repressor DNA complex, J. Am. Chem. Soc. 116 (1994) 6464–6465.
[18] D. Nietlispach, R.T. Clowes, R.W. Broadhurst, Y. Ito, J. Keeler, M. Kelly, J. Ashurst, H. Oschkinat, P.J. Domaille, E.D. Laue, An approach to the structure determination of larger proteins using triple resonance NMR experiments in conjunction with random fractional deuteration, J. Am. Chem. Soc. 118 (1996) 407–415.
[19] K. Pervushin, R. Riek, G. Wider, K. Wuthrich, Attenuated T-2 relaxation by mutual cancellation of dipole–dipole coupling and chemical shift anisotropy indicates an avenue to NMR structures of very large biological macromolecules in solution, Proc. Natl. Acad. Sci. USA 94 (1997) 12366–12371.
[20] R. Ishima, P.T. Wingfield, S.J. Stahl, J.D. Kaufman, D.A. Torchia, Using amide H-1 and N-15 transverse relaxation to detect millisecond time-scale motions in perdeuterated proteins: application to HIV-1 protease, J. Am. Chem. Soc. 120 (1998) 10534–10542.
[21] A. Abragam, Principles of Nuclear Magnetism, Oxford Science Publications, Oxford, 1961.
[22] T.K. Mal, S.J. Matthews, H. Kovacs, I.D. Campbell, J. Boyd, Some NMR experiments and a structure determination employing a N-15,H-2 enriched protein, J. Biomol. NMR 12 (1998) 259–276.
[23] D.M. Briercheck, G.S. Rule, Effect of deuteration on the accuracy of HN–HN distance constraints, J. Magn. Reson. 134 (1998) 52–56.
[24] R. Pachter, C.H. Arrowsmith, O. Jardetzky, The effect of selective deuteration on magnetization transfer in larger proteins, J. Biomol. NMR 2 (1992) 183–194.
[25] J.R. Bright, A.R. Pickford, J.R. Potts, I.D. Campbell, Preparation of isotopically labeled recombinant fragments of fibronectin for functional and structural study by heteronuclear nuclear magnetic resonance spectroscopy, Methods Mol. Biol. 139 (2000) 59–69.
[26] H. Sticht, A.R. Pickford, J.R. Potts, I.D. Campbell, Solution structure of the glycosylated second type 2 module of fibronectin, J. Mol. Biol. 276 (1998) 177–187.
[27] D. Voet, J.G. Voet, Biochemistry, third ed., Wiley, New York, 2003.
[28] T.S. Ulmer, I.D. Campbell, J. Boyd, The effects of dissolved oxygen upon amide proton relaxation and chemical shift in a perdeuterated protein, J. Magn. Reson. 157 (2002) 181–189.
[29] R. Freeman, H.D.W. Hill, Fourier transform study of NMR spin-lattice relaxation by progressive saturation, J. Chem. Phys. 54 (1971) 3367–3377.
[30] C. Bauer, R. Freeman, T. Frenkiel, J. Keeler, A.J. Shaka, Gaussian pulses, J. Magn. Reson. 58 (1984) 442–457.
[31] V. Sklenar, Suppression of radiation damping in multidimensional Nmr experiments using magnetic-field gradients, J. Magn. Reson. Ser. A 114 (1995) 132–135.
[32] L.E. Kay, L.K. Nicholson, F. Delaglio, A. Bax, D.A. Torchia, Pulse sequences for removal of the effects of cross-correlation between dipolar and chemical-shift anisotropy relaxation mechanism on the measurement of heteronuclear T1 and T2 values in proteins, J. Magn. Reson. 97 (1992) 359–375.
[33] J. Boyd, U. Hommel, I.D. Campbell, Influence of cross-correlation between dipolar and anisotropic chemical-shift relaxation mechanisms upon longitudinal relaxation rates of N-15 in macromolecules, Chem. Phys. Lett. 175 (1990) 477–482.
[34] A.J. Shaka, P.B. Barker, R. Freeman, Computer-optimized decoupling scheme for wideband applications and low-level operation, J. Magn. Reson. 64 (1985) 547–552.
[35] A.G. Palmer, N.J. Skelton, W.J. Chazin, P.E. Wright, M. Rance, Suppression of the effects of cross-correlation between dipolar and anisotropic chemical-shift relaxation mechanisms in the measurement of spin spin relaxation rates, Mol. Phys. 75 (1992) 699–711.
[36] N.R. Skrynnikov, R.R. Ernst, Detection of intermolecular chemical exchange through decorrelation of two-spin order, J. Magn. Reson. 137 (1999) 276–280.
[37] G. Lipari, A. Szabo, Model-free approach to the interpretation of nuclear magnetic-resonance relaxation in macromolecules. 1. theory and range of validity, J. Am. Chem. Soc. 104 (1982) 4546–4559.
[38] M. Ottiger, A. Bax, Determination of relative N-H-N N-C′, C-alpha-C′, and C(alpha)-H-alpha effective bond lengths in a protein by NMR in a dilute liquid crystalline phase, J. Am. Chem. Soc. 120 (1998) 12334–12341.
[39] J. Boyd, C. Redfield, Characterization of N-15 chemical shift anisotropy from orientation-dependent changes to N-15 chemical shifts in dilute bicelle solutions, J. Am. Chem. Soc. 121 (1999) 7441–7442.
[40] G. Cornilescu, A. Bax, Measurement of proton, nitrogen, and carbonyl chemical shielding anisotropies in a protein dissolved in a dilute liquid crystalline phase, J. Am. Chem. Soc. 122 (2000) 10143–10154.
[41] D. Fushman, N. Tjandra, D. Cowburn, Direct measurement of N-15 chemical shift anisotropy in solution, J. Am. Chem. Soc. 120 (1998) 10947–10952.
[42] I. Solomon, Relaxation processes in a system of two spins, Phys. Rev. 99 (1955) 559–565.
[43] C.L. Teng, R.G. Bryant, Experimental measurement of nonuniform dioxygen accessibility to ribonuclease a surface and interior, J. Am. Chem. Soc. 122 (2000) 2667–2668.
[44] T.L. Hwang, S. Mori, A.J. Shaka, P.C.M. vanZijl, Application of phase-modulated CLEAN chemical EXchange spectroscopy (CLEANEX-PM) to detect water-protein proton exchange and intermolecular NOEs, J. Am. Chem. Soc. 119 (1997) 6203–6204.
[45] K. Venu, V.P. Denisov, B. Halle, Water H-1 magnetic relaxation dispersion in protein solutions. A quantitative assessment of internal hydration, proton exchange, and cross-relaxation, J. Am. Chem. Soc. 119 (1997) 3122–3134.
[46] Y.W. Bai, J.S. Milne, L. Mayne, S.W. Englander, Primary structure effects on peptide group hydrogen-exchange, Proteins 17 (1993) 75–86.
[47] J. Boyd, N.R. Skrynnikov, Calculations of the contribution of ring currents to the chemical shielding anisotropy, J. Am. Chem. Soc. 124 (2002) 1832–1833.
[48] C.H. Cho, J. Urquidi, S. Singh, G.W. Robinson, Thermal offset viscosities of liquid H2O, D2O, and T2O, J. Phys. Chem. B 103 (1999) 1991–1994.
[49] S.P. Smith, Y. Hashimoto, A.R. Pickford, I.D. Campbell, J.M. Werner, Interface characterization of the type II module pair from fibronectin, Biochemistry 39 (2000) 8374–8381.
[50] M. Goldman, Quantum Description of High-Resolution NMR in Liquids, Clarendon Press, Oxford, 1988.
[51] E.T. Olejniczak, C.M. Dobson, M. Karplus, R.M. Levy, Motional averaging of Proton nuclear overhauser effects in proteins—predictions from a molecular-dynamics simulation of lysozyme, J. Am. Chem. Soc. 106 (1984) 1923–1930.

[52] R. Bruschweiler, B. Roux, M. Blackledge, C. Griesinger, M. Karplus, R.R. Ernst, Influence of rapid intramolecular motion on nmr cross-relaxation rates—a molecular-dynamics study of antamanide in solution, J. Am. Chem. Soc. 114 (1992) 2289–2302.

[53] R. Abseher, S. Ludemann, H. Schreiber, O. Steinhauser, Nmr cross-relaxation investigated by molecular-dynamics simulation—a case-study of ubiquitin in solution, J. Mol. Biol. 249 (1995) 604–624.

[54] J.A. Jones, Optimal sampling strategies for the measurement of relaxation times in proteins, J. Magn. Reson. 126 (1997) 283–286.

[55] A.G. Palmer, M. Rance, P.E. Wright, Intramolecular motions of a zinc finger DNA-binding domain from Xfin characterized by proton-detected natural abundance C-12 heteronuclear Nmr-spectroscopy, J. Am. Chem. Soc. 113 (1991) 4371–4380.

[56] A.M. Mandel, M. Akke, A.G. Palmer, Backbone dynamics of *Escherichia coli* Ribonuclease Hi—correlations with structure and function in an active enzyme, J. Mol. Biol. 246 (1995) 144–163.